Title
Two-Dimensional Near Ultraviolet (2DNUV) Spectroscopic Probe of Structural-Dependent Exciton Dynamics in a Protein

Journal
The Journal of Physical Chemistry B, 119(4)

ISSN
1520-6106

Authors
Li, Jun
Deng, Mingsen
Voronine, Dmitri V
et al.

Publication Date
2015-01-29

DOI
10.1021/jp509314y

Peer reviewed

Two-dimensional Near Ultraviolet (2DNUV) Spectroscopic Probe of Structural-dependent Exciton Dynamics in A Protein

Journal:	*The Journal of Physical Chemistry*
Manuscript ID:	jp-2014-09314y.R2
Manuscript Type:	Article
Date Submitted by the Author:	n/a
Complete List of Authors:	Li, Jun; University of Science and Technology of China, School of Chemistry and Materials Science Deng, Mingsen; Guizhou Provincial Key Laboratory of Computational Nano-Material Science, Voronine, Dmitri; Institute for Quantum Science and Engineering, Department of Physics Mukamel, Shaul; The University of California, Irvine, Department of Chemistry Jiang, Jun; University of Science and Technology of China, School of Chemistry and Materials Science

Two-dimensional Near Ultraviolet (2DNUV) Spectroscopic Probe of Structural-dependent Exciton Dynamics in A Protein

Jun Li,[†] Mingsen Deng,[‡] Dmitri V. Voronine,[¶] Shaul Mukamel,[¶] and Jun Jiang[*,†]

Hefei National Laboratory for Physical Sciences at the Microscale, Collaborative Innovation Center of Chemistry for Energy Materials, School of Chemistry and Materials Science, University of Science and Technology of China, Hefei, 230026, China, Guizhou Provincial Key Laboratory of Computational Nano-Material Science, Institute of Applied Physics, Guizhou Normal College, Guiyang, 550018, China, and University of California Irvine, Chemistry Department, University of California Irvine, California, USA.

E-mail: jiangj1@ustc.edu.cn

[*]To whom correspondence should be addressed

[†]Hefei National Laboratory for Physical Sciences at the Microscale, Collaborative Innovation Center of Chemistry for Energy Materials, School of Chemistry and Materials Science, University of Science and Technology of China, Hefei, 230026, China

[‡]Guizhou Provincial Key Laboratory of Computational Nano-Material Science, Institute of Applied Physics, Guizhou Normal College, Guiyang, 550018, China

[¶]University of California Irvine, Chemistry Department, University of California Irvine, California, USA.

Abstract

Understanding the exciton dynamics in biological systems is crucial for the manipulation of their function. We present a combined quantum mechanics (QM) and molecular dynamics (MD) simulation study that demonstrates how coherent two dimensional near ultraviolet (2DNUV) spectra can be used to probe the exciton dynamics in a mini-protein, Trp-cage. 2DNUV signals originate from aromatic transitions which are significantly affected by the couplings between residues, which determine exciton transport and energy relaxation. The temporal evolution of 2DNUV features captures important protein structural information, including geometric details and peptide orientations.

Keywords: Two dimensional near ultraviolet spectroscopy (2DNUV), Exciton dynamics, Quantum mechanics (QM), Molecular dynamics (MD)

I. Introduction

Stimulated by the importance of understanding and controlling energy flow and dissipation processes in biological systems,[1] exciton dynamics in biomolecules has long been under active studies.[2,3] Probing exciton dynamics in proteins is essential for fundamental cell biology as well as for protein engineering. However, it has never been an easy task, mainly due to the fact that the exciton behaviors are dictated by the quantum mechanism and rely on molecular interactions, which vary a lot during biological functions and are hardly accessible to traditional techniques. Coherent ultrafast two-dimensional (2D) spectroscopy has emerged as complementary to nuclear magnetic resonance (NMR) that determines protein geometry from structural-dependent chemical shifts.[4] The 2D infrared spectroscopy (2DIR) has been proven to be a powerful tool in identifying the local geometric details of protein.[5,6] 2D electronic spectroscopic signal is coming from the transition of electrons which is often globally distributed and coupled effectively with the electrostatic potential of surroundings, and thereby carries rich information of molecular interactions and reflects both local and global

protein structures under environmental fluctuation. It is also known that the transition and migration of electrons are much faster than atoms. Therefore, UV signals induced by electron excitation of protein can capture the temporal evolution of excitons before the geometric changes of proteins. 2D electronic spectroscopy offers direct access to the exciton structure and dynamics of chromophore aggregates by spreading spectral information over two or more frequency axes.[5–8] 2D signals carry information of molecular interactions, including exciton couplings, chemical exchange, coherence transfer, spectral diffusion, and system-bath interactions, and their temporal evolution provides a direct probe of the structural-dependent exciton dynamics.[9–11]

Here we studied the two-dimensional near ultraviolet (2DNUV) spectra of a model system, the trp-cage protein. This is a mini-protein with 20 amino acids. The folded peptide has a tryptophan (trp) residue located inside the cage of other residues, so the optical signals of this trp residue carry geometric and kinetic information of the whole protein. The electronic transitions of the trp and tyrosine (tyr) aromatic residues form a simple excitonic system in the near ultraviolet (NUV: 250 $\sim$ 300 nm) region. The two dominant aromatic transitions have a small energy difference (< 3000 cm^{-1}), ensuring strong coupling and making exciton dynamics detectable. Such small energy difference also meets the realistic bandwidth of ultrafast UV lasers, so that 2D experimental measurement is feasible.[12–14] One can thus follow the temporal evolution of photon echoes and capture the dynamics of exciton population relaxation. Meanwhile, the directions of aromatic transition dipoles are nearly fixed in the aromatic residue, so their interactions with polarized laser pulses reflect protein orientation. This would contribute to the study of protein anisotropy which is important for drug design. We have carried out a combined quantum mechanics (QM) and molecular dynamics (MD) simulation for 2DNUV signals of the trp-cage protein induced by four coherent ultrashort time-ordered laser pulses. By varying the time delay between the second and third pulses, we followed the temporal evolution of the 2D signal which reflects the exciton dynamics. The QM and MD simulation protocol also enables us to examine the dependence of exciton

dynamics on molecular interactions, which is hardly accessible to traditional techniques.

II. Theoretical methods

The trp-cage structure

Neidigh *et. al.*[15] have designed a series of trp-cage proteins, among which TC5b was widely studied. The TC5b trp-cage consists of 20-residue with the sequence of "NLYIQWLKDGG PSSGRPPPS", in which there are only two aromatic side chains: the sixth trp residue (Trp6) and the third tyr residue (Tyr3). The structure of TC5b is displayed in Fig. 1 (A), in which the backbone trace is shown as a ribbon, the side chains are depicted with wires, and the aromatic chains Tyr3 and Trp6 are highlighted with tubes. The Trp6 is located inside the cage of all other residues.

Aromatic transitions

The transition energies, electric and magnetic dipole moments of isolated aromatic chromophores are calculated by QM CASSCF/SCRF (the complete-active space self-consistent-field)[16] method implemented within a self-consistent reaction field in MOLCAS.[17] The excitation energies of NUV transitions of three aromatic amino acids are given in Table 1. In the NUV region (250 $\sim$ 300 nm, 33333 $\sim$ 40000 cm^{-1}), only the $^1\mathrm{L}_b$ transition of Tyr3 (labeled as Yb), and the $^1\mathrm{L}_b$ and $^1\mathrm{L}_a$ transition of Trp6 (labeled as Wb and Wa) contribute to optical signals.

Table 1: Computed excited state energies $\varepsilon_{me,0}$ for the isolated benzene, phenol and indole in the NUV region.

$\varepsilon_{me,0}$ (cm^{-1})	$^1\mathrm{L}_b$	$^1\mathrm{L}_a$
benzene	38005	47953
phenol	36492	46205
indole	35396	38053

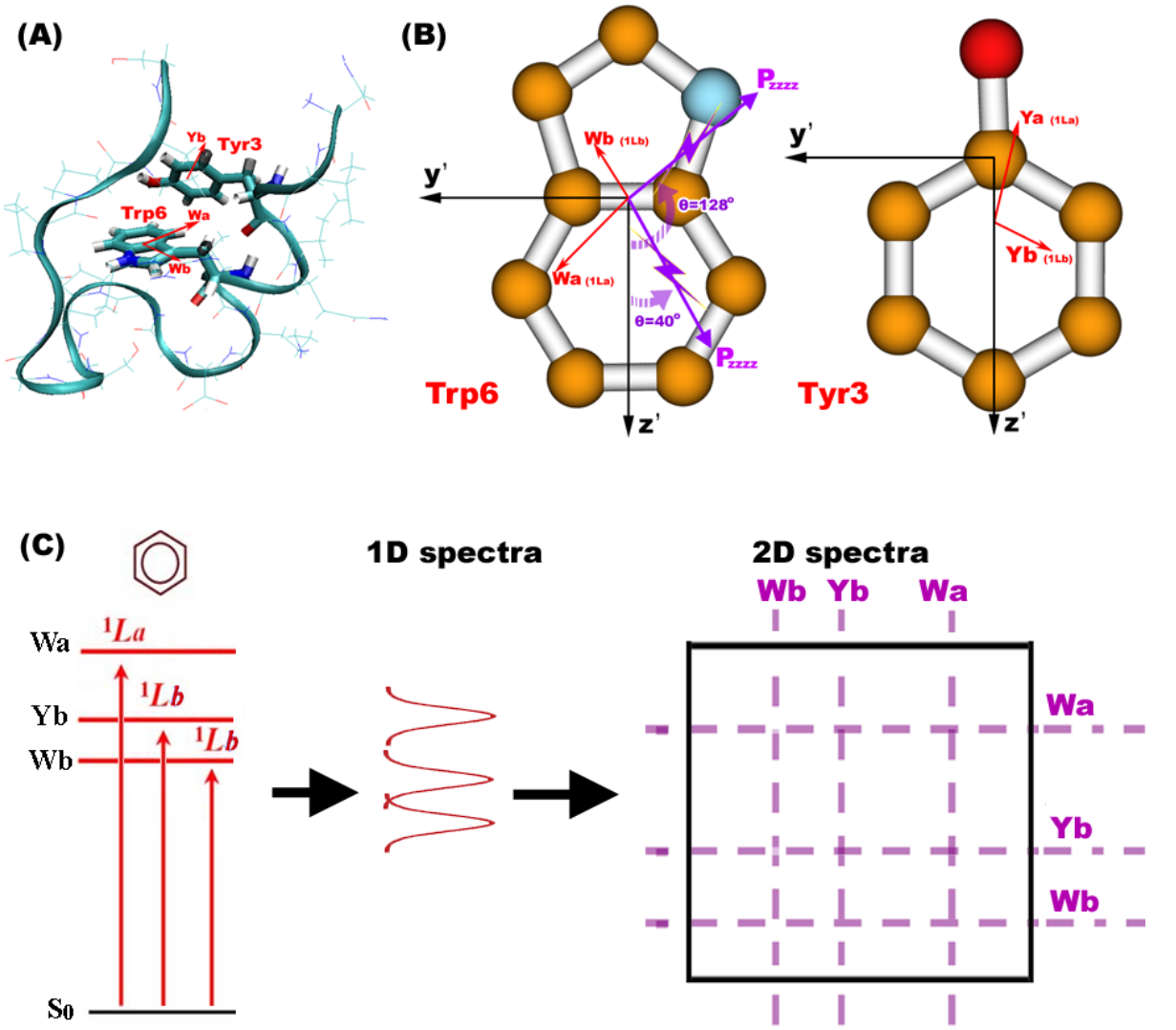

Figure 1: (A): TC5b trp-cage structure. Trp6s located inside the cage. (B): The indole fragment of Trp6 whose benzene ring is located on the y'-z' plane of Cartesian space x'y'z' with the Trp6 center C-C bond parallel to y' axis . The phenol fragment of Tyr3 with the benzene plane on the y'-z' plane. The electric dipoles of Wa and Wb transitions are depicted with red arrows, and the polarizations of Pzzzz UV laser pulses are shown as purple arrows. (C): The excitonic energy diagram composed of Wa and Wb transitions of Trp6, and Yb transition of Tyr3, which contribute to photon echo signals in 1D and 2D spectra.

The aromatic chromophores of Trp6 and Tyr3 are displayed in Fig. 1 (B), red arrows represent the electric dipoles of the Wb, Yb, and Wa transitions. The electric dipole of Wa (^1L_a) is along the short axis of the aromatic ring, while that of Wb and Yb (^1L_b) is along the long axis. The electric dipoles of ^1L_a and ^1L_b are perpendicular to each other in one chromophore, and their magnetic dipoles are perpendicular to the aromatic ring. These three dipole vectors of Wa, Wb, and Yb can decide the three-dimensional space. Three transitions form a simple excitonic energy diagram as illustrated in Fig. 1 (C). Their photo-responses to polarized laser pulses carry abundant structural information of the trp-cage peptide. The population relaxation from higher to lower energy levels should dominate the exciton dynamics.

Quantum mechanics and Molecular mechanics simulations

Starting geometric coordinates of the TC5b trp-cage were taken from the RSCB protein data bank (PDB code: 1L2Y). MD simulations were carried out using the software package NAMD 2.7[18] with the CHARMM27[19] force field and the TIP3P water model.[20] We employed the NPT ensemble, and cubic periodic boundary conditions. The particle mesh Ewald sum method was used to treat the long-range electrostatics. A non-bonded cutoff radius of 12 $\mathring{A}$ was used. Ensembles of molecular dynamics (MD) geometric snapshots were recorded for 16 ns dynamics after 2 ns of equilibration at 1 atm pressure and 310 K. Structures of 1000 MD snapshots with the 400 fs interval were extracted for the UV studies. It is found that 1000 snapshots produce identical 2DUV signals as 1500 snapshots, demonstrating the data convergence. Meanwhile, our previous work of 2DUV on the same protein have shown that the correlation between MD snapshots will not affect the 2DUV signal evolutions.[21]

The proteins are divided into fragments of amino acids and peptide bond units. The fragments were then saturated by hydrogen terminations. The excited and ground states of isolated fragments are computed with QM methods. The aromatic chromophores Trp and Tyr are modeled by CASSCF/SCRF and CASPT2 calculations of the indole and phenol

molecules, respectively. The gas-phase electronic structures and charge densities of all amino acids and water molecules were obtained with the hybrid DFT B3LYP/6-311++G** method implemented in the GAUSSIAN03 package.[22] It is true that we perform MD simulations and later calculate some fragments (active chromophore groups) of the resulting snapshots at the QM level.

Our exciton Hamiltonian with electrostatic fluctuations (EHEF)algorithm is used to combine the QM and MD outputs, and construct effective exciton Hamiltonian with electrostatic fluctuations.[23,24] EHEF enables us to calculate the electrostatic potential, inter- and intramolecular interactions, and the corrected transition energies under environmental fluctuations at the QM level for each MD snapshot. Based on the Frenkel model, the matrix method in DichroCalc program[25,26] uses the parameters from EHEF to build Hamiltonian. By doing this, we focused on the photo-response of active chromophore groups (peptide bonds and aromatic rings). The contributions of the rest of protein are considered by the interactions between their ground state electrostatic potential and the excitation transition densities of active chromophore groups.

The 2D photon echo signal

Based on the exciton Hamiltonian, UV spectra were simulated using the SPECTRON code.[27] The full inhomogeneous UV spectra are obtained by averaging over all MD snapshots. The 2DNUV signal is generated by four impulsive coherent short laser pulses, labeled by their wavevectors $\mathbf{k}_1$, $\mathbf{k}_2$, $\mathbf{k}_3$, and $\mathbf{k}_4$, with $\mathbf{k}_4 = -\mathbf{k}_1 + \mathbf{k}_2 + \mathbf{k}_3$. The absorption change of the $\mathbf{k}_4$ beam is recorded as a function of the three consecutive delay times: t_1, t_2, and t_3. Here 2D signals are calculated by two-dimensional Fourier transform $t_1 \rightarrow \Omega_1$ and $t_3 \rightarrow \Omega_3$ with t_2 varying. In this work, we focus on the non-chiral 2D signal, so the zzzz polarization configuration for four laser pulses (*i.e.* the $\mathbf{k}_1$, $\mathbf{k}_2$, $\mathbf{k}_3$, $\mathbf{k}_4$ laser pulses with polarizations along the z axis as illustrated in Fig. 1 (B)) is used. Four Gaussian laser pulses are centered at 37000 cm^{-1}($\sim$270 nm) with full width at half maximum (FWHM) bandwidth 3000 cm^{-1}

(∼24nm). We used the protocol described in ref.[28] When two excitons generated by electronic transitions approach the same chromophore, they scatter due to Pauli exclusion. We have used the nonlinear exciton equations (NEE) approach and the scattering matrix is built as described in ref.[28] This method avoids the diagonalization of doubly excited states and can be used in large proteins with hundreds of units. Signals are plotted using non-linear scale which reveals both the strong and weak features,

$$\text{arcsinh}(c\mathbf{S}) = \ln(c\mathbf{S} + \sqrt{1 + c^2\mathbf{S}^2}), \tag{1}$$

The signal $\mathbf{S}$ is multiplied by a scale factor c to make it close to 1, so that weak amplitudes are amplified: for $c\mathbf{S}< 1$ the scale is linear, $\text{arcsinh}(c\mathbf{S}) \approx c\mathbf{S}$, and for larger $c\mathbf{S}$ it becomes logarithmic, $\text{arcsinh}(c\mathbf{S}) \approx (\mathbf{S}|\mathbf{S}|^{-1})ln(2|c\mathbf{S}|)$.

Exciton population relaxation is simulated with the Red Field relaxation matrix for single-exciton space population-coherence dynamics.[6] With the quasi-particle model,[29,30] interactions between excitons on peptide and environment bath are characterized by the oscillation of transition energies under environmental fluctuations. The distributions of oscillators for the Wb, Yb, Wa transitions found in 1 ns dynamics are displayed in Fig. 2 (A). Obviously, the strongest transition Wa has the broadest and most complicated distribution pattern for oscillators, while the Yb distribution is very sharp. The correlation function of the n-th transition mode in the real space at time t can be calculated with

$$C_n(t) = \frac{< \Delta E_n(t) - \Delta E_n(\infty) >}{< \Delta E_n(0) - \Delta E_n(\infty) >} \tag{2}$$

where $\Delta E_n(t)$ represents the energy shift induced by environment interactions, and was computed for 120, 000 MD snapshots with the 8 fs interval. And $\Delta E_n(\infty)$ was calculated by averaging with all MD snapshots. Here <> means three trajectories were averaged to consider the dynamic ensemble. The correlation functions $C_n''(\omega)$ in the frequency domain

were obtained through the Fourier transform of $C_n(\tau)$, as we have

$$C_n(t) = \int \frac{d\omega}{2\pi} e^{-i\omega t}[1 + coth(\beta\hbar\omega)/2]C''(\omega) \quad (3)$$

The correlation functions for three modes are displayed in Fig. 2 (B). Corresponding to oscillator distributions, the Wa transition holds the strongest oscillations.

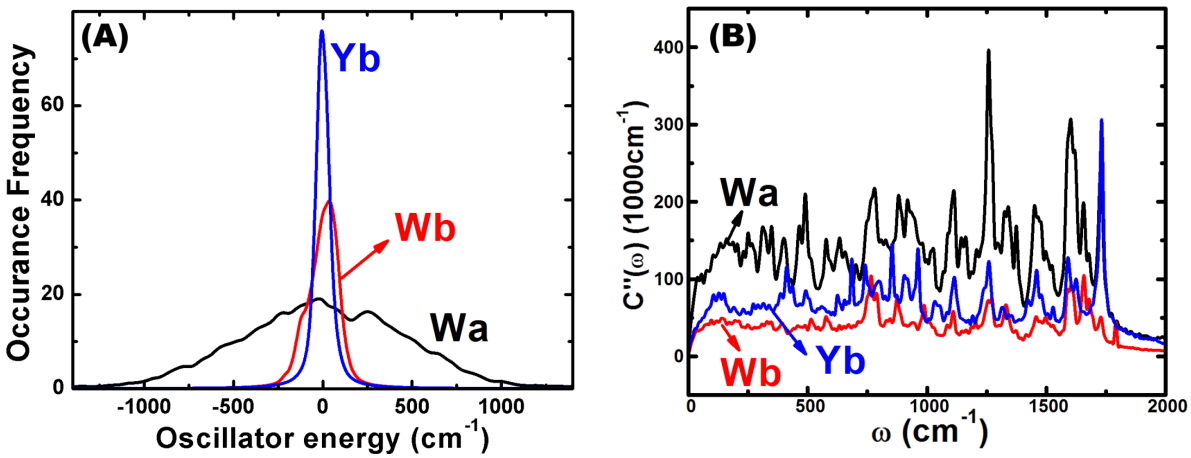

Figure 2: (A) The distribution of oscillator strength and (B) the correlation functions of the Wb, Yb, Wa transitions obtained from 120,000 MD snapshots with the 8 fs interval.

III. Results and Discussion

CD spectra

Conventional 1D spectroscopic techniques such as linear absorption (LA) and circular dichroism (CD) are widely used to identify protein structures and calibrate theoretical simulations. [31] Our simulated LA and CD spectra of the TC5b trp-cage in the far-ultraviolet (FUV, 190∼250 nm) and NUV (250∼300 nm) region are displayed in Fig. 3. FUV are induced by protein backbone transitions. The FUV LA spectrum in Fig. 3 (A) is dominated by three absorption peaks. The longest wavelength peak (∼223 nm) is induced by the protein backbone $n \longrightarrow \pi^*$ transitions, while the highest peak at the short wavelength (∼192 nm)

corresponds to the $\pi \longrightarrow \pi^*$ transitions. Because of the Davydov splitting effect, the helical structure in TC5b have a split fraction of $\pi \longrightarrow \pi^*$ transitions at lower energy frequency and produce the absorption peak at ∼207 nm. CD spectra carry richer characteristic information of protein secondary structure. Our simulated FUV CD spectrum in Fig. 3 (B) exhibits good agreement with reported experimental CD results, showing two negative peaks at 223 and 207 nm, and strong positive signals at around 192 nm. Three dominant CD peaks in experiments as denoted by Exp1[32] and Exp2[15] are repeated by simulations. It is known that two negative CD peaks in the region of 200 239 nm together with one positive peak at around 190 nm resemble the typical CD feature of α-helix secondary structure.

NUV optical signals reflect the excitations and couplings of Wa, Yb, and Wb transitions. Their frequencies are marked with dashed lines in the NUV LA and CD spectra displayed in Fig. 3 (C) and (D). In the LA spectrum, Wa, Yb and Wb transitions produce absorption peaks at ∼261, 274, and 282 nm, respectively. And the couplings between Wa and Yb result in an extra absorption peak at ∼268 nm. The simulated NUV CD spectrum is compared to experiment in Fig. 3 (D). NUV signal induced by aromatic transitions are normally very weak, so the experimental NUV CD (denoted Exp1)[32] in Fig. 3 (D) was measured for the trp-cage sample with protein concentration 20 times higher than the one used in Exp1 FUV CD measurement in Fig. 3 (B). This explains why we had to scale down Exp1 NUV CD intensities for 20 times to get a reasonable comparison in signal intensity magnitude with our simulated CD. It is found by simulations that strongly coupled transitions of aromatic residues always lead to positive NUV CD signals. In measuring the Exp1 NUV CD in Fig. 3 (D), the abnormally high protein concentrations have largely enhanced the interactions and couplings between the aromatic rings, resulting in very strong positive CD signals. This is very different to the situations in both our simulations and the Exp1 FUV CD spectra measurement when the trp-cage is in normal protein concentration. We thus need to take into account of the strong positive background CD signals for the NUV CD of Exp1 in comparing with our computation results. Nevertheless, in the simulated NUV CD in Fig. 3 (D), Wa,

Yb, Wb transitions produce three negative valleys at 261, 274, and 282 nm superimposing the negative background signals (from 200 to 300 nm) of the backbone. Neglecting the background signals of the backbone, the simulated NUV CD actually agrees well with the Exp1 NUV CD.

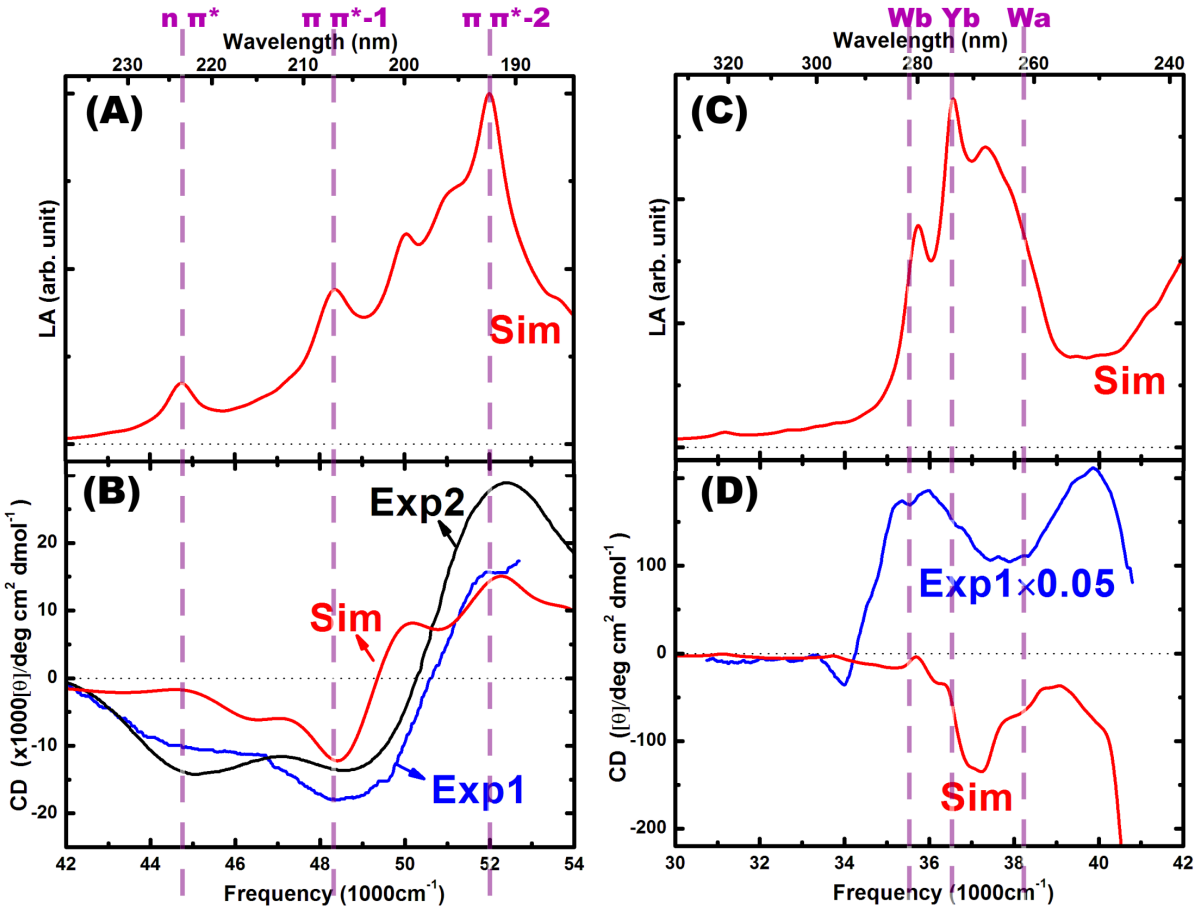

Figure 3: LA (top panel) and CD (bottom panel) spectra in the FUV (left column) and NUV (right column) region. Red curves are simulated results averaged over 1000 MD snapshots, blue and black CD curves are taken from reported experiments Exp1[32] and Exp2,[15] and purple dashed lines mark dominant optical signals induced by three electronic transitions. FUV LA and CD signals are dominated by three transitions at around 223, 207, and 192 nm, resembling the typical CD feature of α-helix secondary structure. NUV LA and CD signals are contributed by the Wa, Yb, Wa transitions, in which the discrepancy between experimental and simulated CD is due to the abnormally strong aromatic couplings from high protein concentration in Exp1[32] NUV CD measurement.

2DNUV for residue-dependent exciton dynamics

2DNUV spectra with the zzzz laser pulse polarization configuration were simulated.[28] We first considered the isotropic orientation with averaged ensemble. The 2DNUV zzzz spectra of trp-cage in the native form (Nat) for time delay t_2= 0 and 10 ps are displayed in the left column of Fig. 4. The Wa, Yb, Wb transitions are marked with vertical and horizontal dashed lines. The 2DNUV spectrum at t_2=0 is dominated by a negative (blue) diagonal peak centered near (Wa+Yb)/2 ($\sim$ 37000 cm^{-1}), suggesting strong couplings between Wa and Yb transitions. The peak decays due to couplings and shifts to the diagonal point at Yb after t_2=10 ps. Consequently, a cross-peak emerges at $\omega_1 \sim$ Wa and $\omega_3 \sim$ Yb frequencies (Wa-Yb). These reflect the exciton population relaxation from Wa to Yb.

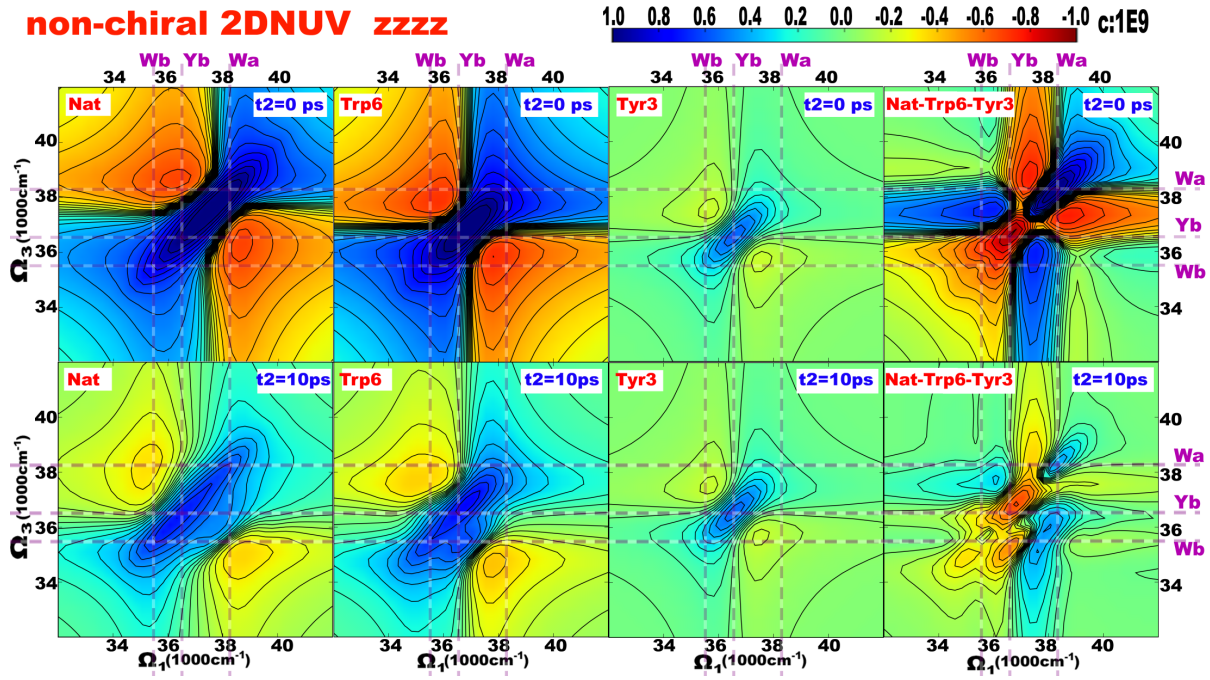

Figure 4: From left to right: simulated 2DNUV zzzz spectra of the isotropic ensembles of the Nat TC5b trp-cage, spectra contributed only by Trp6 and Tyr3, and difference spectra Nat-Trp6-Tyr3 after t_2=0 ps (the top panel) and 10 ps (the top panel) time delay. Purple dashed lines mark the Wa, Yb, and Wb transitions. Scale factor c and magnitude bar are shown above.

To display the excitons kinetics, 2DNUV spectra of Trp6 (Wa and Wb transitions)

and Tyr3 (Yb transition) residues are computed and displayed in Fig. 4. Signals coming from isolated Trp6 or Tyr3 are much weaker than those of Nat TC5b, demonstrating that residue couplings significantly enhance photon echo response. The static spectrum of Trp6 at t_2=0 exhibits a dominant diagonal peak centered at the middle of Wa and Wb frequencies, which also decays with t_2 time increasing. At t_2=10 ps, a cross peak is observed at $\omega_1 \sim$ (Wa+Wb)/2 and $\omega_3 \sim$ Wb, reflecting the energy relaxation from Wa to Wb. Tyr3 has only one Yb transition and no exciton couplings in the NUV region, so one can barely see the decay of its diagonal peak even after 10 ps time delay.

In order to identify the signals induced by residue couplings between Trp6 (Wa and Wb) and Tyr3 (Yb), the difference spectra of Nat-Trp6-Tyr3 (subtracting Trp6 and Tyr3 contributions from Nat signals) were displayed in the right column of Fig. 4. 2DNUV at t_2=0 shows one negative (blue) diagonal peak at the Wa frequency and one positive (red) diagonal peak at the Yb frequency, both of which decay with t_2 increasing. At t_2=10 ps, the cross peaks of Wa and Yb (Wa-Yb), Wa and Wb (Wa-Wb), Yb and Wb (Yb-Wb) are clearly resolved in the difference spectrum. These demonstrate that residue couplings are responsible for the population relaxation from higher to lower energy level.

The temporal evolution of some dominant 2DNUV peaks are plotted in Fig. 5. The diagonal peaks in the Nat and Trp6 spectra decay exponentially with the increase of time, while their cross peaks increase exponentially. The exponential decay rule was widely used to explain the temporal evolution of 2D signals.[33,34] Here our simulated 2DNUV signals follow a triexponential decay trend. Using a function of $S = S_0 + c_1\exp(-t_2/\tau_1) + c_2\exp(-t_2/\tau_2) + c_3\exp(-t_2/\tau_3)$, we have obtained fitted curves in good agreement with the computed results in Fig. 5. The fitted parameters of three decay rates are listed in Table. 2. The τ_1 with values close to 0.03 ps and τ_2 in sub-ps scale should account for the fast decay by the intrinsic exciton dephasing process and environmental interactions, respectively, as they have nearly the same values for different transition modes (Wa, Yb, Wb) and three protein residue compositions (Nat, Trp6, Tyr3). In contrast, the value of τ_3 in several ps scale increases dramatically

from the Nat to isolated Trp6 and Tyr3 spectra, so it should describe the exciton decay due to electronic transition couplings. The order of τ_3 value is Nat < Trp6 < Tyr3, suggesting that couplings between transitions facilitate the population relaxations and shorten exciton lifetime.

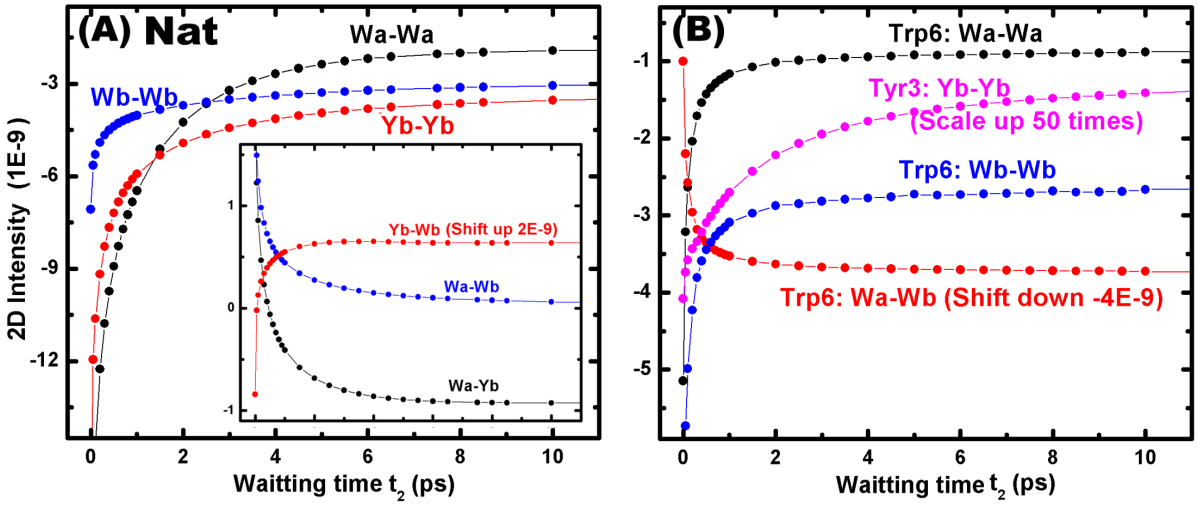

Figure 5: The evolution of peak intensity as the function of the t_2 time delay in the Nat (A) and Trp6 (Tyr3) (B) 2DNUV zzzz spectra. The square dots represent computed intensity values, and solid lines are fitted with the triexponential decay function.

Table 2: The fitted decay rates (ps) of the triexponential decay function for the diagonal and cross peaks of the Nat, Trp6 and Tyr3 non-chiral 2DNUV zzzz spectra.

	Nat						Trp6			Tyr3
	Wa-Wa	Yb-Yb	Wb-Wb	Wa-Yb	Wa-Wb	Yb-Wb	Wa-Wa	Wb-Wb	Wa-Wb	Yb-Yb
τ_1	0.037	0.025	0.027	0.028	0.028	0.027	0.033	0.032	0.031	0.028
τ_2	0.26	0.28	0.29	0.23	0.26	0.21	0.27	0.30	0.25	1.30
τ_3	1.61	2.27	3.15	1.39	2.02	0.62	5.10	6.76	4.51	8.60

2DNUV for geometry-dependent exciton dynamics

Peptide geometry determines the residue coupling, which influences light-induced exciton dynamics. As in the trp-cage structure in Fig. 1 (B), the angle ϕ between the Yb and Wb

(Wa) dipoles are key parameters to determine the peptide geometry. Based on the mass center of the trp and tyr residue, we can define the distance and relative angle between Yb and Wb (Wa) transitions. Based on 60, 000 MD snapshots, the distance and coupling energies between the Yb and Wb (Wa) transitions are plotted as the function of the transition dipole angle ϕ_{Yb-Wb} (ϕ_{Wa-Yb}) in the left panel of Fig. 6 (Fig. 7). The Yb-Wb distance has a linear dependence on cos[2(ϕ_{Yb-Wb}-10^o)]. The shift of 10 degree in the distance-angle dependence behavior imply the effect of other geometric factors such as the dihedral angle. In principle, the coupling intensity (energy) between two dipoles μ_1 and μ_2 is proportion to $\mu_1 \cdot \mu_2$. Therefore, we found that the Yb-Wb coupling intensity is a linear function of sin[4ϕ_{Yb-Wb}], as shown in Fig. 6 (B). As the decay of 2DNUV signals are strongly affected by residue couplings, their temporal evolutions should be sensitive to the change of the dipole angles. As expected, the change of spectral intensities from 0 to 10 ps t_2 time delay for three 2DNUV peaks (Yb-Yb, Wb-Wb, Yb-Wb) in Fig. 6 (C), depend linearly on sin[4(ϕ_{Yb-Wb}-10)]. Meanwhile, Fig. 7 (A) shows that the distance between Wa and Yb transitions is independent to their dipole angle ϕ_{Wa-Yb}. As a result, the couplings between Wa and Yb in Fig. 7 (B), and the difference spectral intensities of the Wa-Wa, Yb-Yb, and Wa-Yb 2DNUV peaks after 10 ps time delay in Fig. 7 (C) exhibit linear dependencies on the function of cos[2ϕ_{Wa-Yb}]. The relationships between 2DNUV signals and dipole angles thus demonstrate the geometry dependence of exciton dynamics.

2DNUV signals for orientation-dependent exciton dynamics

Fig. 1 (A) shows that the Wb and Wa transition dipoles of the Trp6 residue are nearly perpendicular. This can be used to examine exciton dynamics in regard to the peptide orientation. As in Fig. 1 (B), we have built a partially oriented peptide ensemble, by rotating every MD snapshot to ensure the aromatic ring of Trp6 on the y'-z' plane of Cartesian space x'y'z' with the Trp6 center C-C bond parallel to y' axis. We then employed four laser pulses with polarization all along the z axis (Pzzzz) to interact with the oriented ensemble as in

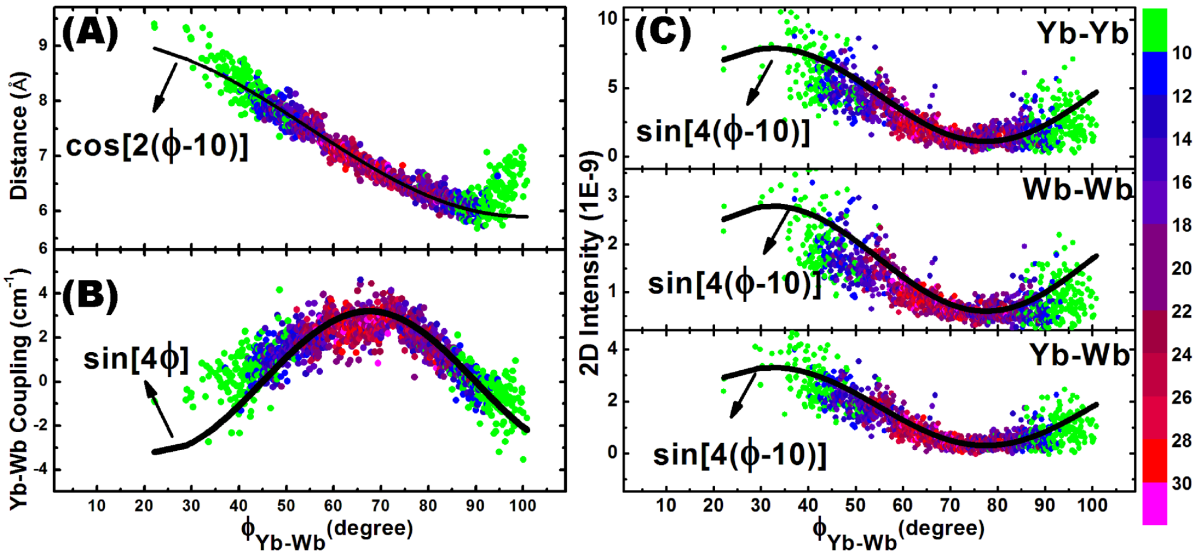

Figure 6: The distance (A) and coupling intensity (B) of the Yb and Wb transitions in the Tc5b trp-cage as the function of their dipole angle (ϕ_{Yb-Wb}). (C) The dependence of the intensity changes from 0 to 10 ps t_2 time delay for three 2DNUV peaks Yb-Yb, Wb-Wb, and Yb-Wb on the dipole angle. Colors from green to red represent the occurrence frequencies in 60, 000 MD snapshots.

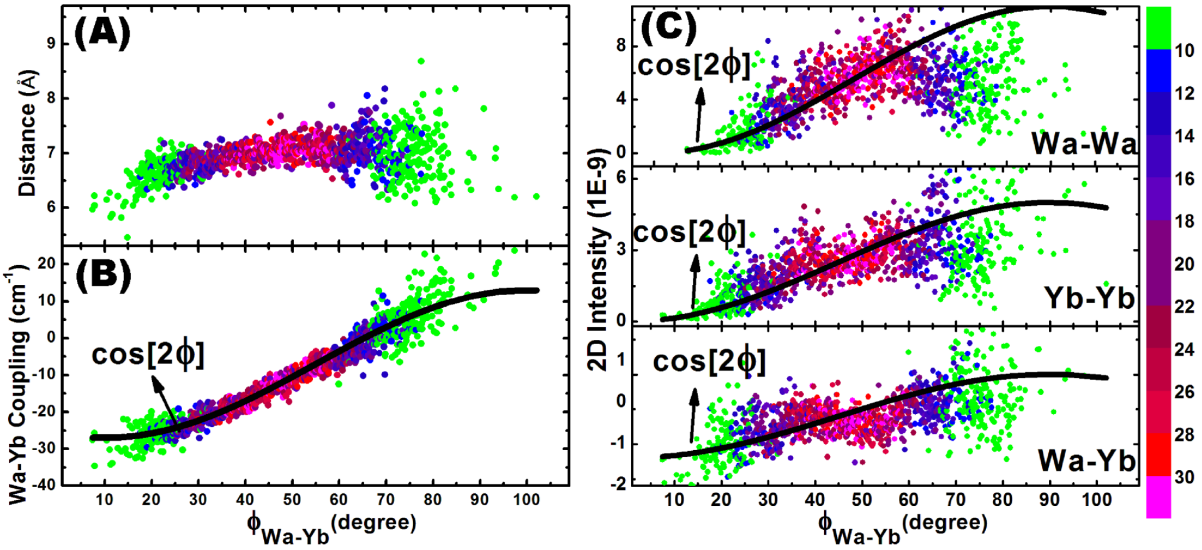

Figure 7: The distance (A) and coupling intensity (B) of the Wa and Yb transitions in the Tc5b trp-cage as the function of the dipole angle (ϕ_{Wa-Yb}). (C) The dependence of the intensity changes from 0 to 10 ps t_2 time delay for three 2DNUV peaks Wa-Wa, Yb-Yb, and Wa-Yb on the dipole angle. Colors from green to red represent the occurrence frequencies in 60, 000 MD snapshots.

Fig. 1 (B). The angle between the laser polarization (z axis) and the z' axis in Cartesian space is denoted as θ. We tuned the polarizations of laser pulses to excite the projections of the Wb and Wa transitions at different directions, and calculated the orientation-dependent 2DNUV signals. For instance, with θ=~40 and ~128 degrees, the laser pulses interact only with the Wb and Wa transitions, respectively. The 2DNUV spectra at 0 and 10 ps time for θ=30, 90, 120, 180 degree are displayed in Fig. 8. In the cases of θ=30 and 120 degree, the Wa and Wb transitions becomes very weak, respectively. The miss of one transition impede the exciton dynamics, as we see no cross peaks after 10 ps time delay. In contrast, a strong cross-peak of Wa-Wb appears after 10 ps time delay when θ=180 in the right of Fig. 8, implying the projections of Wa and Wb transitions on the laser polarization direction has reached a good balance.

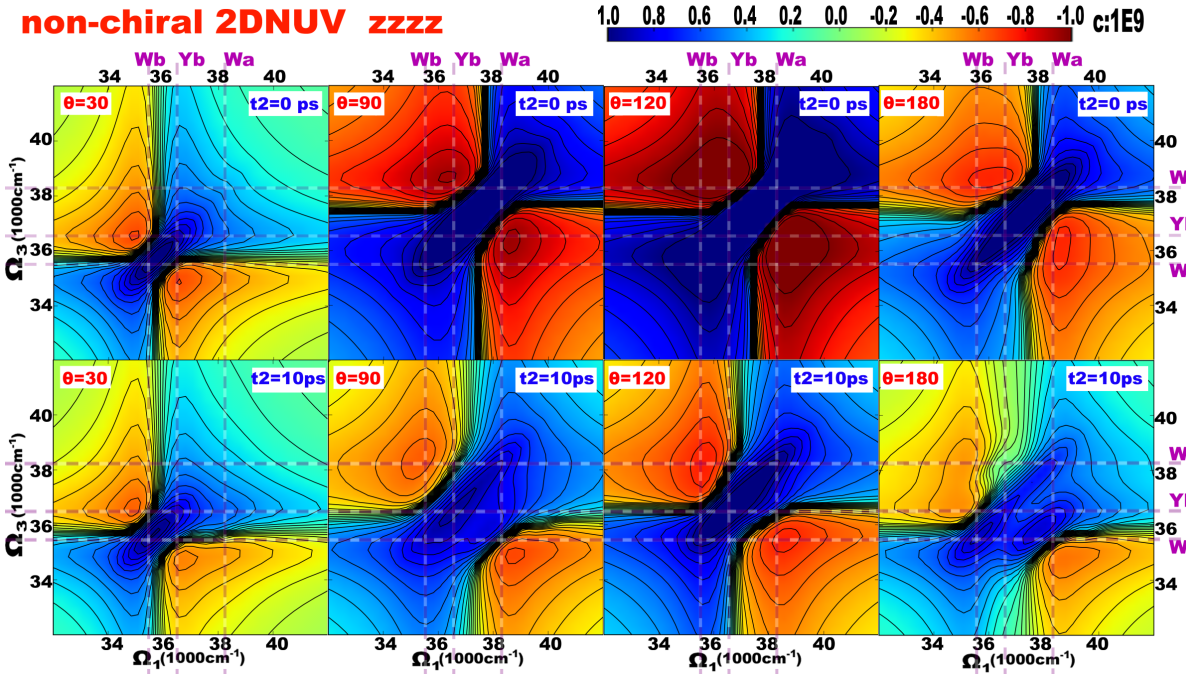

Figure 8: Simulated 2DNUV zzzz spectra of a native Tc5b trp-cage protein with orientation angle θ=30, 90, 120, 180 degree (from left to right) after t_2=0 ps (the top panel) and 10 ps (the bottom panel) time delay of energy relaxation. Purple dashed lines mark dominant optical signals and corresponding electronic transitions. Scale factor c and magnitude bar are shown above.

The temporal evolutions of 2DNUV signals of an oriented ensemble follow the triexpo-

nential decay rule. It is found that the decay rates rely on the θ angle. It is too complicated to extract a clear mathematical relationship between the decay of 2DNUV signals and the θ angle, implying there are multiple factors. On the other hand, the decay of 2DNUV Wa-Wb cross peak exhibits clear trigonometric dependence. The fitted values of τ_1, τ_2, and τ_3 rates for Wa-Wb evolutions are plotted as the function of θ from 0 to 180 degree in Fig. 9. It is interesting to note that these three rates are proportion to the function of sin[2θ].

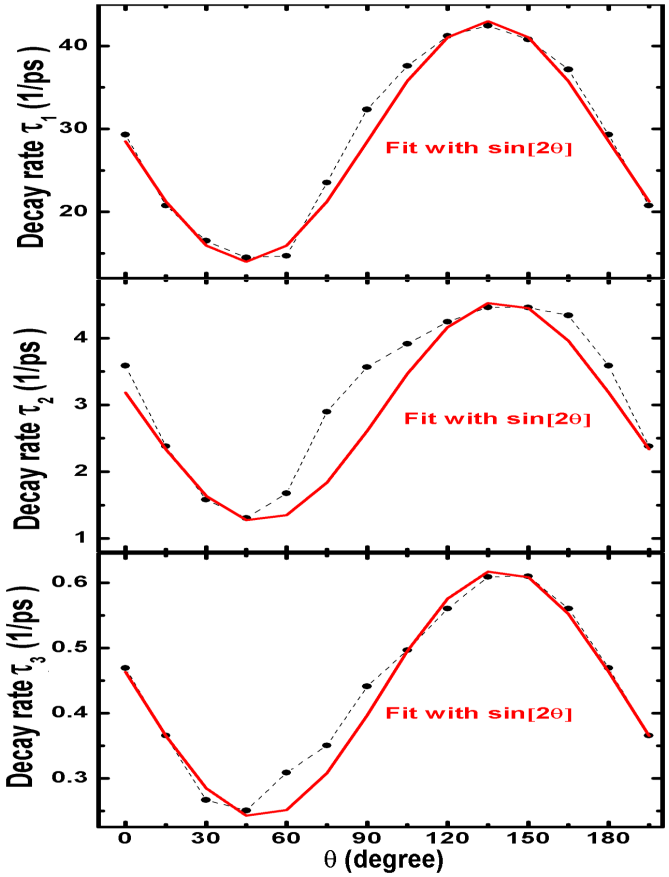

Figure 9: The decay rates the 2DNUV Wa-Wb cross peak as the function of θ (angle between laser polarizations and the z' axis of the indole of the Trp6 residue in Fig. 1 (B)). Black dots and dashed lines stand for fitted decay rates, and red solid curves are fitted with the function of sin[2θ].

IV. Conclusions

In summary, we have used the temporal evolution of 2DNUV spectra to study the structural-dependent exciton dynamics in a model protein. We demonstrated that the exciton transport and energy relaxation rate depend on the structural parameters of the protein, such as the geometric details and peptide orientations. These would be very useful for the structural determination of proteins, and reveal some crucial structure-property relationships. One can also expect some anisotropy of motions and allosteric behavior in proteins, which will help understand and manipulate biochemically relevant interactions such as ligand binding so that facilitate related drug designs.

Acknowledgments We gratefully acknowledge the support of the CAS Strategic Priority Research Program B (No. XDB01020000), National Natural Science Foundation of China (Grant 21473166, 91221104), Recruitment Program of Global Experts of China, Fundamental Research Funds for the Central Universities (WK2090050027, WK2310000035), and Program for Innovative Research Team of Guizhou Province of China (QKTD-[2012]4009).

References

(1) Lee, H.; Cheng, Y.-C.; Fleming, G. Coherence Dynamics in Photosynthesis: Protein Protection of Excitonic Coherence. *Science* **2007**, *316*,1462–1465.

(2) Arndt, M.; Juffmann, T.; Vedral, V. Quantum Physics Meets Biology. *HFSP J.* **2009**, *3*,386–400.

(3) Schrodinger, E. *What Is Life? The Physical Aspect of The Living Cell;* Cambridge University Press, 1944.

(4) Cavalli, A.; Salvatella, X.; Dobson, C. M.; Vendruscolo, M. Protein Structure Determination from NMR Chemical Shifts. *Proc. Natl. Acad. Sci. USA* **2007**, *104*, 9615–9620.

(5) Ostroumov, E. E.; Mulvaney, R. M.; Cogdell, R. J.; Scholes, G. D. Broadband 2D

Electronic Spectroscopy Reveals a Carotenoid Dark State in Purple Bacteria. *Science* **2013**, *340*, 52–56.

(6) Mukamel, S.; Abramavicius, D.; Yang, L.; Zhuang, W.; Schweigert, I. V.; Voronine, D. Coherent Multidimensional Optical Probes for Electron Correlations and Exciton Dynamics: From NMR to X-rays. *Acc. Chem. Res.* **2009**, *42*, 553–562.

(7) Engel, G. S.; Calhoun, T. R.; Read, E. L.; Ahn, T. K.; Mančal, T.; Cheng, Y. C.; Blankenship, R. E.; Fleming, G. R. Evidence for Wavelike Energy Transfer through Quantum Coherence in Photosynthetic Systems. *Nature* **2007**, *446*, 782–786.

(8) Brixner, T.; Stenger, J.; Vaswani, H. M.; Cho, M.; Blankenship, R. E.; Fleming, G. R. Two-dimensional Spectroscopy of Electronic Couplings in Photosynthesis. *Nature* **2005**, *434*, 625–628.

(9) Consani, C.; Aubock, G.; van Mourik, F.; Chergui, M. Ultrafast Tryptophan-to-Heme Electron Transfer in Myoglobins Revealed by UV 2D Spectroscopy. *Science* **2013**, *339*, 1586–1589.

(10) Jiang, J.; Mukamel, S. Two-Dimensional Ultraviolet (2DUV) Spectroscopic Tools for Identifying Fibrillation Propensity of Protein Residue Sequences. *Agnew Chem. Int. Ed.* **2010**, *49*, 9666–9669.

(11) Jiang, J.; Golchert, K. J.; Kingsley, C. N.; Brubaker, W. D.; Martin, R. W.; Mukamel, S. Exploring the Aggregation Propensity of γS-Crystallin Protein Variants Using Two-Dimensional Spectroscopic Tools. *J. Phys. Chem. B.* **2013**, *117*, 14294–14301.

(12) West, B. A.; Womick, J. M.; Moran, A. M. Probing Ultrafast Dynamics in Adenine With Mid-UV Four-Wave Mixing Spectroscopies. *J. Phys. Chem. A*. **2011**, *115*, 8630–8637.

(13) Tseng, C.; Matsika, S.; Weinacht, T. Two-Dimensional Ultrafast Fourier Transform Spectroscopy in The Deep Ultraviolet. *Opt. Express* **2009**, *17*, 18788–18793.

(14) Nuernberger, P.; Selle, R.; Langhojer, F.; Dimler, F.; Fechner, S.; Gerber, G.; Brixner, T. Polarization-shaped Femtosecond Laser Pulses in The Ultraviolet. *J. Opt. A: Pure Appl. Opt.* **2009**, *11*, 085202.

(15) Neidigh, J.; Fesinmeyer, R. M.; Andersen, N. H. Designing A 20-residue Protein. *Nat.Struc. Bio.* **2002**, *9*, 425–30.

(16) Yamamoto, N.; Vreven, T.; Robb, M.; Frisch, M.; Schlegel, H. A Direct Derivative MC-SCF Procedure. *Chem. Phys. Lett.* **1996**, *250*, 373–378.

(17) Aquilante, F.; Vico, L. D.; Ferré, N.; Ghigo, G.; Malmqvist, P.-A.; Neogrády, P.; Pedersen, T. B.; Pitonák, M.; Reiher, M.; Roos, B. O.; Serrano-Andrés, L.; Urban, M.; Veryazov, V.; Lindh, R. MOLCAS 7: The Next Generation. *J. Comput. Chem.* **2009**, *31*, 224–247.

(18) Phillips, J.; Braun, R.; Wang, W.; Gumbart, J.; Tajkhorshid, E.; Villa, E.; Chipot, C.; Skeel, R.; Kalé, L.; Schulten, K. Scalable Molecular Dynamics with NAMD. *J. Comput. Chem.* **2005**, *26*, 1781–1802.

(19) MacKerell, Jr., A. D.; Bashford, D.; Bellott, M.; Dunbrack, Jr., R. L.; Evanseck, J. D.; Field, M. J.; Fischer, S.; Gao, J.; Guo, H.; Ha, S.; Joseph-McCarthy, D.; Kuchnir, L.; Kuczera, K.; Lau, F. T. K.; Mattos, C.; Michnick, S.; Ngo, T.; Nguyen, D. T.; Prodhom, B.; Reiher, III, W.; Roux, B.; Schlenkrich, M.; Smith, J. C.; Stote, R.; Straub, J.; Watanabe, M.; Wiorkiewicz-Kuczera, J.; Yin, D.; Karplus, M. All-Atom Empirical Potential for Molecular Modeling and Dynamics Studies of Proteins. *J. Phys. Chem. B* **1998**, *102*, 3586–3616.

(20) Jorgensen, W. L.; Chandrasekhar, J.; Madura, J. D.; Impey, R. W.; Klein, M. L.

Comparison of Simple Potential Functions for Simulating Liquid Water. *J. Chem. Phys.* **1983**, *79*, 926–935.

(21) Jiang, J.; Zaizhi, L.; Jin, W.; Mukamel, S. Signatures of The Protein Folding Pathway in Two-Dimensional Ultraviolet Spectroscopy. *J. Phys. Chem. Lett.* **2014**, *5*, 1341–1346.

(22) Gaussian 03, revision c.02. Frisch, M. J.; Trucks, G. W.; Schlegel, H. B.; Scuseria, G. E.; Robb, M. A.; Cheeseman, J. R.; Montgomery, J. J. A.; Vreven, T.; Kudin, K. N.; Burant, J. C.; Millam, J. M.; Iyengar, S. S.; Tomasi, J.; Barone, V.; Mennucci, B.; Cossi, M.; Scalmani, G.; Rega, N.; Petersson, G. A.; Nakatsuji, H.; Hada, M.; Ehara, M.; Toyota, K.; Fukuda, R.; Hasegawa, J.; Ishida, M.; Nakajima, T.; Honda, Y.; Kitao, O.; Nakai, H.; Klene, M.; Li, X.; Knox, J. E.; Hratchian, H. P.; Cross, J. B.; Bakken, V.; Adamo, C.; Jaramillo, J.; Gomperts, R.; Stratmann, R. E.; Yazyev, O.; Austin, A. J.; Cammi, R.; Pomelli, C.; Ochterski, J. W.; Ayala, P. Y.; Morokuma, K.; Voth, G. A.; Salvador, P.; Dannenberg, J. J.; Zakrzewski, V. G.; Dapprich, S.; Daniels, A. D.; Strain, M. C.; Farkas, O.; Malick, D. K.; Rabuck, A. D.; Raghavachari, K.; Foresman, J. B.; Ortiz, J. V.; Cui, Q.; Baboul, A. G.; Clifford, S.; Cioslowski, J.; Stefanov, B. B.; Liu, G.; Liashenko, A.; Piskorz, P.; Komaromi, I.; Martin, R. L.; Fox, D. J.; Keith, T.; Al-Laham, M. A.; Peng, C. Y.; Nanayakkara, A.; Challacombe, M.; Gill, P. M. W.; Johnson, B.; Chen, W.; Wong, M. W.; Gonzalez, C.; Pople, J. A. **2004**.

(23) Jiang, J.; Abramavicius, D.; Bulheller, B. M.; Hirst, J. D.; Mukamel, S. Ultraviolet Spectroscopy of Protein Backbone Transitions in Aqueous Solution: Combined QM and MM Simulations. *J. Phys. Chem. B* **2010**, *114*, 8270–8277.

(24) Jiang, J.; Mukamel, S. Two-dimensional Near-ultraviolet Spectroscopy of Aromatic Residues in Amyloid Fibrils: A First Principles Study. *Phys. Chem. Chem.Phys.* **2010**, *13*, 2394–2400.

(25) Hirst, J. D. Improving Protein Circular Dichroism Calculations in The Far-ultraviolet

through Reparametrizing The Amide Chromophore. *J. Chem. Phys.* **1998**, *109*, 782–788.

(26) Bulheller, B. M.; Rodger, A.; Hirst, J. D. Circular and Linear Dichroism of Proteins . *Phys. Chem. Chem. Phys.* **2007**, *9*, 2020–2035.

(27) Abramavicius, D.; Palmieri, B.; Voronine, D. V.; Šanda, F.; Mukamel, S. Coherent Multidimensional Optical Spectroscopy of Excitons in Molecular Aggregates; Quasiparticle versus Supermolecule Perspectives. *Chem. Rev.* **2009**, *109*, 2350–2408.

(28) Abramavicius, D.; Jiang, J.; Bulheller, B. M.; Hirst, J. D.; Mukamel, S. Simulation Study of Chiral Two-Dimensional Ultraviolet Spectroscopy of The Protein Backbone. *J. Am. Chem. Soc.* **2010**, *132*, 7769–7775.

(29) Palmieri, B.; Abramavicius, D.; Mukamel, S. Interplay of Slow Bath Fluctuations and Energy Transfer in 2D Spectroscopy of The FMO Light-harvesting Complex: Benchmarking of Simulation Protocols. *Phys. Chem. Chem. Phys.* **2010**, *12*, 108–114.

(30) Rivalta, I.; Nenov, A.; Cerullo, G.; Mukamel, S.; Garavelli, M.; Ab Initio Simulations of Two-dimensional Electronic Spectra: The SOS//QM/MM Approach. *Int. J. Quantum Chem.* **2014**, *114*, 85–93.

(31) Rogers, D. M.; Hirst, J. D. First-Principles Calculations of Protein Circular Dichroism in The Near Ultraviolet. *Biochemistry* **2004**, *43*, 11092–11102.

(32) Adams, C. M.; Kjeldsen, F.; Patriksson, A.; van der Spoel, D.; Graslund, A.; Papadopoulos, E.; Zubarev, R. A. Probing Solution- and Gas-phase Structures of Trp-cage Cations by Chiral Substitution and Spectroscopic Techniques. *J. Mass Spectrom* **2006**, *253*, 263–273.

(33) Nee, M. J.; Baiz, C. R.; Anna, J. M.; McCanne, R.; Kubarych, K. J. Multilevel Vibra-

tional Coherence Transfer and Wavepacket Dynamics Probed with Multidimensional IR Spectroscopy. *J. Chem. Phys.* **2008**, *129*, 084503.

(34) Panitchayangkoon, G.; Voronine, D. V.; Abramavicius, D.; Mukamel, S.; Engel, G. S. Direct Evidence of Quantum Transport in Photosynthetic Light-harvesting Complexes. *Proc. Natl. Acad. Sci. USA* **2011**, *108*, 20908–20912.

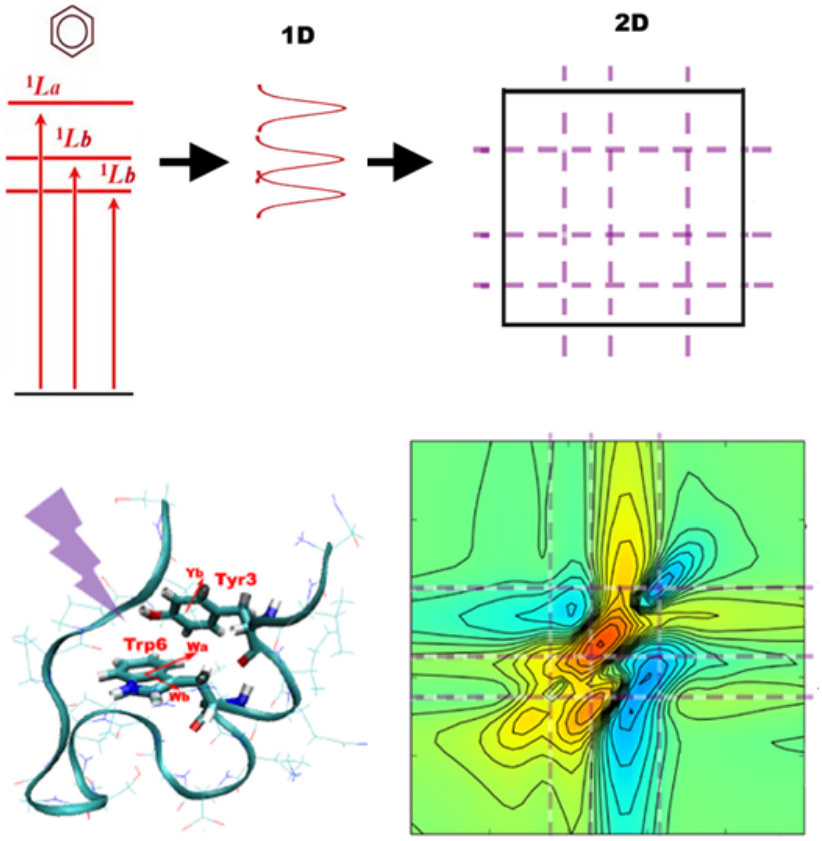

Figure 10: Table of Contents